A Comprehensive Oxide-Based ReRAM TCAD Model with Experimental Verification

W. Goes[1], D. Green[1], P. Blaise[1], G. Piccolboni[2], A. Bricalli[2], A. Regev[3], G. Molas[4], J.-F. Nodin[4]
[1]Silvaco Europe, Compass Point St. Ives, Cambridgeshire, PE275JL, UK, email: wolfgang.goes@silvaco.com
[2]Weebit-Nano France, Grenoble Cedex 9, France, email: {gpiccolboni/alessandro}@weebit-nano.com
[3]Weebit-Nano, Hod Hasharon, Israel, email: amir@weebit-nano.com
[4]CEA-Leti, Grenoble Cedex 9, France, email: {gabriel.molas/jean-francois.nodin}@cea.fr

***Abstract*—**During the last few years, oxide-based ReRAM technology has attracted intense industrial and scientific research interest. Therefore, we have performed an in-depth computational study with a focus on data retention besides the resistive switching and the current run-away. Our newly developed comprehensive TCAD (Technology Computer Aided Design) model provides deep insight into the underlying microscopic processes and is validated against experimental data as an accurate and predictive simulation tool.

I. Introduction

Oxide-based ReRAM is an emerging memory technology that combines the advantages of both RAM and Flash technologies [1-4]. With the increasing demand for big data, artificial intelligence, and neuromorphic computing, ReRAM will play an important role in meeting future memory requirements. For optimizing this technology, predictive and physics-based TCAD simulations are vital as they can dramatically speed up the design, fabrication, and commercial use of new microelectronic technologies through the elimination of expensive and time-consuming experimental test wafers during technology adoption. So far, a few research groups have already undertaken interesting modeling attempts [4-8], which provided first microscopic insight behind the resistive switching. However, their fundamental works focused on the role of oxygen vacancies and interstitials during the SET, RESET, and forming operations alone [4-7]. In this work, we extend the ReRAM investigations to data retention while accounting for the frequently neglected impact of the current compliance on the device characteristics. For this purpose, we make use of the versatile applicability of the generic chemistry module in Silvaco's Victory TCAD package [9] and validated a new ReRAM model against experimental measurements supplied by Weebit-nano.

II. Experimental Devices

The electrical data for this work were obtained using Weebit-nano's oxide-based ReRAM [3] made in Leti facility in Grenoble France. The non-stoichiometric silicon oxide (SiO_x) was chosen as a switching material for non-volatile memories due to its manufacturability ease and its good switching properties. Fig. 1 represents a SEM cross section of the memory stack integrated on top of a 130nm-technology CMOS (back end of line technology). The inset of Fig. 1 shows the stack composition: TiN bottom electrode (BE), SiO_x active layer, and Ti top electrode (TE) acting as oxygen-scavenging layer [10]. The devices studied in this work are single cells in 1 transistor-1 resistor (1T1R) configuration where the transistor is used as current limiter. The SiOx layer was processed using two different deposition techniques and, accordingly, the devices are referred to as type-A or type-B devices in this paper. The processed devices require an electro-forming operation to create a conductive filament (CF) between the two electrodes, which can be disrupted and re-created by RESET and SET operations, respectively. A typical I(V) curves for both SET and RESET operations are depicted in Fig. 2.

III. TCAD Model

Bulk reaction: Over the last few years, the ReRAM technology has attracted increasing interest in understanding these devices on a microscopic level. A special focus has been on the properties of the non-stoichiometric SiO_x and defects therein. Similar to amorphous silicon dioxide, the atomic SiO_x network shows a wide distribution of bond lengths and angles, giving rise to large site-to-site variations in the local material properties and consequently an increased occurrence of defect-like structures. Therefore, it is supposed to contain appreciable amounts of defects or precursor sites. One such a defect, called weak site (D_{ws}) in this work, is a Frenkel pair which becomes electrically active upon the application of high electric fields and decays into a doubly-charged oxygen vacancy (V_O) and a doubly-charged oxygen interstitial (I_O).

$$D_{\mathrm{ws}} \leftrightarrow V_0^{2+} + I_0^{2-} \qquad (1)$$

This electro-forming reaction has been invoked in several studies [5-7]. In our simple model (see Fig. 3 left), we employ the formulation of the thermochemical model [5-7] for the reaction rates (see Fig. 4). The first product of the electro-forming reaction is the V_O, which is present in its positive charge state. In many studies [5], the V_O is assumed to be immobile due to a high diffusion barrier, which is related to the neutralization of V_O by electron capture. V_O can also carry an inelastic trap-to-trap tunneling current [6-7,11], giving rise to a higher conductivity due an increased V_O density. This conduction mechanism is a quite complex process and is phenomenologically described by an extended bridging mobility model (see Fig. 5), which has already been successfully used for CBRAM applications [12]. The I_O, the other product of the electro-forming reaction, is negatively charged and mobile within the oxide. Its transport [13] is described by the ion continuity equation (see Fig. 4), which is solved self-consistently together with the reaction equations, the Poisson equation, the ion continuity equations for I_O and D_{ws}, the electron continuity equation, and the lattice heat flow equation. The latter is considered to account for heating effects associated with the current run-away of ReRAM devices.

Interface reaction and catalyst effects: The interface at the BE is intransparent for the I_O as the TiN is known to be a chemically inert material. By contrast, the Ti TE is reactive and, therefore, assumed to undergo field-dependent reactions which bond or release I_O during the operation of the ReRAM device (see Fig. 3).

$$T_{\mathrm{If}} + I_{\mathrm{O}}^{2-} \leftrightarrow T_{\mathrm{IfO}}^{2-} \quad (2)$$

Here, T_{if} and T_{ifo} are trapping sites for I_O in its oxidized and unoxidized state, respectively. The corresponding reaction rates are of the same form as the electro-forming reaction but for the interface reaction equation.

The electro-forming reaction along with the interface reaction correspond to the basic ReRAM model. In an extended version of this model (see Fig. 3 right), the interface reaction involves a catalyst (C_f).

$$T_{\mathrm{If}} + I_{\mathrm{O}}^{2-} + C_f \leftrightarrow T_{\mathrm{IfO}}^{2-} + C_f \quad (3)$$

Even though the exact nature of this catalyst is unknown, a likely candidate could be some sort of hydrogen [14], which is ubiquitously present during the fabrication. This hydrogen is assumed to be trapped at a lattice site but can be released by a field-dependent reaction and subsequently accelerate the interface reaction. To speed up the computation, we do not solve the continuity equation for the catalyst species but account for their field-dependent concentration by an additional factor as explained in Fig. 4.

Mixed-mode: Due to the unwanted run-away current, real devices are protected using a current compliance. As this strongly affects the physical and chemical processes in the ReRAM devices, the current compliance is modeled as a transistor in a mixed-mode simulation. This combined circuit and device simulation environment has been implemented into Silvaco's commercial TCAD tool Victory Device [9] in order to enable comprehensive studies of ReRAM devices.

IV. Simulation Results

Both the simple as well as the extended ReRAM model are evaluated against Weebit's experimental current hysteresis data of the type-A and the type-B ReRAM devices. In those measurements, the bias at the TE were slowly ramped in the quasi-static regime. The obtained hysteresis curves are smooth and, therefore, well suited for a comparison to the simulation results as no statistical analysis is required. In the simulated device, we assume a two-dimensional simulation domain with a radial symmetry for the filamentary region. An initial condition of 10^{19} cm^{-3} weak spots is used, decreasing from the center of the device. In order to rule out any spurious transient effects due to an incorrect initial distribution of the involved chemical species, we perform a long initial equilibration step at room temperature and zero bias. In a subsequent transient simulation, the TE voltage is repeatedly cycled between −1.3V and +1.3V using linear bias ramps. In analogy to the short SET and RESET operations, the slow quasi-static bias sweeps will be denoted as SET forward/backward and RESET forward/backward in the following.

SET phase: The simulation results of the simple and the extended (see Table 1) model are shown in Fig. 6 and Fig.7, respectively, and both are found to be in good agreement with the experimental data. Below 0.8V, the weak spots remain stable and the current is dominated by the resistivity of the pristine oxide. At higher biases, the electro-forming reaction sets in and generates I_O and V_O (see Fig. 8). The latter form the CF associated with the low-resistance state (LRS). As the trap-to-trap conduction mechanism is inelastic, heat is generated within the oxide during the SET as well as the RESET phase (see Fig. 9). This triggers a positive-feedback loop between the thermally activated trap-to-trap tunneling current and the heating of the CF. The current compliance, however, prevents this run-away effect by limiting the electric field across the oxide at a sufficiently low level (see Fig. 10). The I_O drift towards the TE interface, where they accumulate and bond to interface defect sites. Even though this reaction has a relatively high energy barrier, it can be overcome due to the high electric field. During the subsequent SET backwards phase, the CF remains stable because the I_O are effectively locked in at the interface and are not available for the reverse mode of the electro-forming reaction.

RESET phase: During this phase, the negative bias at the TE is ramped up. This leads to an increase in the current and the heat generation, similar as in the SET forward phase. Due to the opposite polarity of the electric field and the increased device temperature (and the catalyst in the case of the extended model), the reverse mode of the interface reaction is activated. The electric field pushes the I_O back into the bulk oxide towards the TE where they recombine with V_O to weak spots (see Fig. 11). This results in the rupture of the CF and the ReRAM device switching back into its high-resistance state (HRS). During the RESET backward phase, an increasing amount of released I_O completely dissolves the disrupted CF.

Retention: In order to study the retention of the LRS, we store the state of the device after the SET phase and perform a long transient simulation at a TE bias of 0V. While the simple model correctly reproduces the current hysteresis, it predicts retention times of less than ~10^8s, despite of intense efforts to optimize the model parameters. As a comprehensive ReRAM model must be capable of explaining long data retention, we also studied the impact of a possible catalytic reaction within the framework of the extended ReRAM model. For this purpose, we evaluate the simple and the extended model against the mean-time-to-failure (MTTF), which has been determined from a large collection of type-B samples (see Fig. 12). The MTTF simulations show that the simple model predicts too short LRS retention times. The extended model, however, yields realistic LRS retention times and correctly reproduce their temperature dependence. The longer retention times in Fig. 12 can be explained by the fact that the field-dependent catalyst concentration in the extended model allows for the smaller interface reaction rates at low biases. The smaller reaction rates hold back the I_O at the TE interface and, with this, the CF and the current through the ReRAM remains stable for long retention times.

V. Conclusion

We have developed a quantitative TCAD model, which accounts for the physical and chemical key mechanisms involved in the resistive switching of ReRAM devices. In particular, our simulations consider the correct treatment of the current compliance and thereby considerably enhances the predictive capability of our simulations. The validity of this new model has been confirmed by a comparison against the electrical characteristics of commercially developed devices from Weebit. Furthermore, the model can also explain long data retention typical for ReRAM devices. As such, this ReRAM model provides a suited tool to investigate the different operation modes of oxide-based ReRAM technologies.

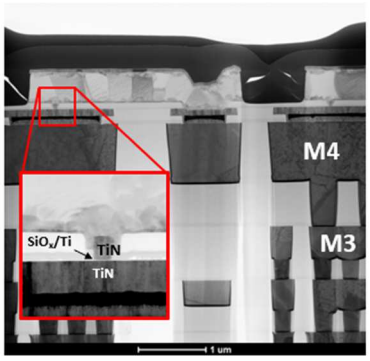

Fig. 1. SEM image of SiO_X-based ReRAM integrated on top of 130nm CMOS. The few nanometer thick SiO_x is sandwitched between TiN at the BE and Ti at the TE.

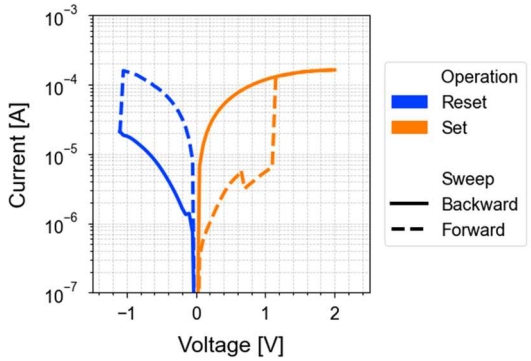

Fig. 2. An exemplary I(V) curve of a type-B sample. The measured device shows a pronounced current hysteresis during the whole SET (orange) and RESET (blue) cycle.

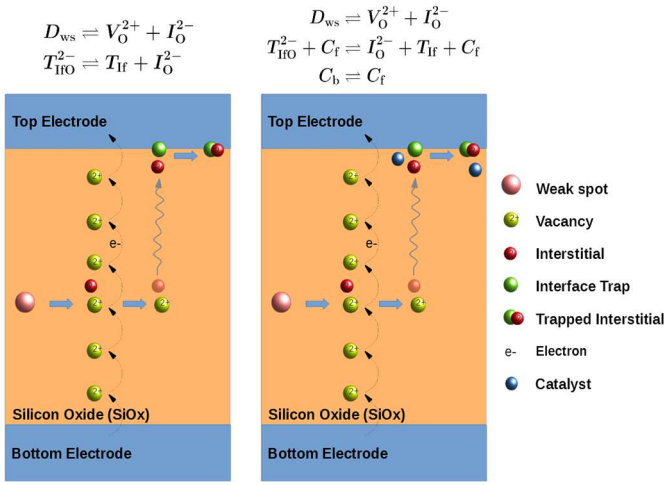

Fig. 3. Physical and chemical processes considered in the simple (left) and the extended (right) ReRAM model. Both models are based on pre-existing weak spots, which decay into I_O and V_O at high electric fields. The V_O are immobile and allow for trap-to-trap tunneling if present in high defect densities. The I_O can diffuse within the SiO_x and even react with interfacial traps at the TE. This simple model is extended by a catalyst species, which is neither created nor consumed by the interface reaction but increases the reaction rates. The catalyst species is assumed to be bonded (C_b) to the SiO_x network but can be released (C_f) by a high electric field.

(a) Species Continuity Equation:

$$\frac{\partial [X]}{\partial t} = -D_X \nabla \left\{ \left(\frac{z_O q_0}{k_b T} \right) [X] \boldsymbol{E} + \nabla [X] \right\} + (G_X - R_X) \quad (1)$$

$$[X] = V_O^{2+},\ I_O^{2-}, D_{ws} \qquad D_X = D_{I_O^{2-}} \quad (2)$$

$$G_{V_O^{2+}} = G_{I_O^{2-}} = R_{D_{ws}} = k_f [D_{ws}] \exp\left(- \frac{E_{bf} \pm \frac{2+k}{3} x\, z\, \boldsymbol{p_0}\, \boldsymbol{E}}{k_B T} \right) \quad (3)$$

$$R_{V_O^{2+}} = R_{I_O^{2-}} = G_{D_{WS}} = k_r [V_O^{2+}]\,[I_O^{2-}] \exp\left(- \frac{E_{br} \mp \frac{2+k}{3}(1-x)\, z\, \boldsymbol{p_0}\, \boldsymbol{E}}{k_B T} \right) \quad (4)$$

$$f_c = \exp\left(- \frac{\boldsymbol{p_1}\, \boldsymbol{E}}{k_b T} \right) \quad (5)$$

(b) Extended Bridging Mobility Model:

$$\mu_{\text{eff}} = \mu_s + w(\delta, f_0)\,[\mu_c \exp(-E_b/k_B T) - \mu_s] \quad (6)$$

Fig. 4. (a) Species continuity equation used to describe the chemistry of V_O, I_O, and D_{WS} in SiO_x. D_X is the corresponding species diffusivity. z and q_0 denote the species charge and elementary charge, respectively. As the V_O and the D_{WS} are assumed to be immobile, their corresponding flux terms vanish. The symbols in square brackets denote the corresponding species concentrations. E_{bf} and E_{br} are the forward and the reverse barrier of the electro-forming reaction at zero field. E is the electric field. $\boldsymbol{p_0(2+k)/3}$ corresponds to the bond polarization factor with k being the dielectric constant. x specifies the location of the saddle point of the barrier as a fraction of the reaction coordinate. The rates of the interface reaction are of the same form as (3) and (4), In the extended ReRAM model, they are multiplied by the factor f_c in order to account for the field-dependent concentration of the catalyst species. (b) The extended bridging mobility model used to describe the electron transport through the oxide. μ_s is the mobility of the host material and μ_c is the increased mobility due to inelastic trap-to-trap tunneling. w denotes a weighing factor for the trap-to-trap tunneling and f_0 is the fraction of the defects at which the conductivity starts to rise.

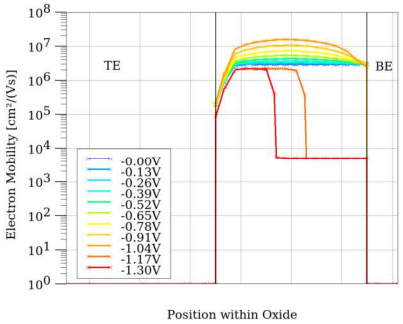

Fig. 5. Extended bridging mobility during the RESET phase. The bias sweep from 0V to -1.3V is represented by the color gradient from the blue to the red color. During the early RESET phase, the device heats up, leading to faster trap-to-trap tunneling. This is reflected in an increased electron mobility. Later during the RESET phase the CF is disrupted at the BE (right-hand side), resulting in a decreased mobility. As in [5], the heat generation is described by Joule heating.

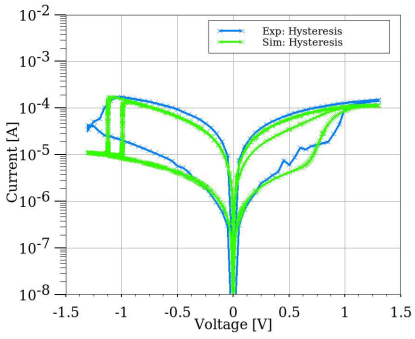

Fig. 6. Comparison of the simulated (green curve) and experimental (blue curve) SET and RESET phase for the simple model. The simulation results nicely match with the experimental data and is therefore consistent with the experimental hysteresis data. The simulations include two full cycles in order to demonstrate the repeatable hysteresis behavior.

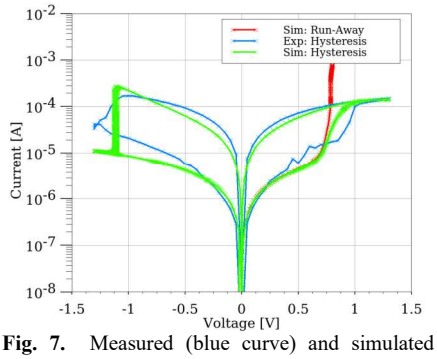

Fig. 7. Measured (blue curve) and simulated (green curve) current hysteresis of a ReRAM for the extended model. The simulation results agree well with the experimental data, demonstrating the validity of this model. The simulation also predicts the current run-away, depicted by the red curve. Note that the involvement of the catalyst allows for an increased barrier of the interface reaction.

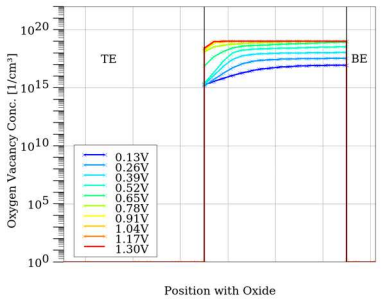

Fig. 8. The V_O profile during the SET forward phase. In agreement with the thermodynamic model, the V_O concentration rises and reaches its maximum values around 0.8V. The high density goes hand in hand with a reduction of the trap-to-trap tunneling length and reflects the formation of the CF.

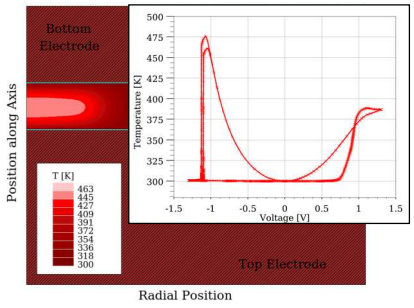

Fig. 9. Temperature profile in the ReRAM device during the RESET phase. This figure demonstrates that the oxide heats up at high voltages. The inset shows that the maximum temperature within the interface layer during the whole current hysteresis. During RESET, the temperature can reach values up to ~175°C.

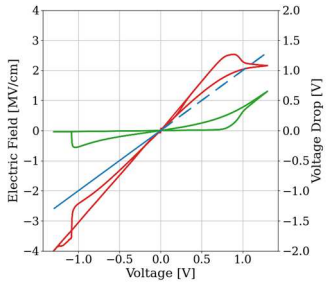

Fig. 10. The potential drop at the compliance transistor (green curve) and at the compliance transistor plus the ReRAM (blue dashed curve). During the SET phase, the applied voltage mainly drops at the ReRAM below 0.8V. Above this value, the CF has been formed with a saturating electric field across the oxide (red curve). This effect strongly impacts the field-dependent chemical processes within the ReRAM.

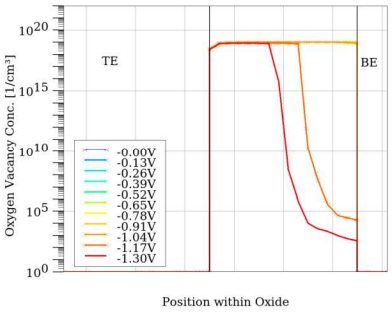

Fig. 11. The V_O concentration during the RESET forward phase. Due to the electric field, the high temperature, and the catalyst, the I_O are released from the TE (left-hand side) and drift towards the BE (right-hand side), where they recombine with V_O to re-form D_{WS}. This is reflected in the rupture of the CF and the return of the ReRAM device to its HRS.

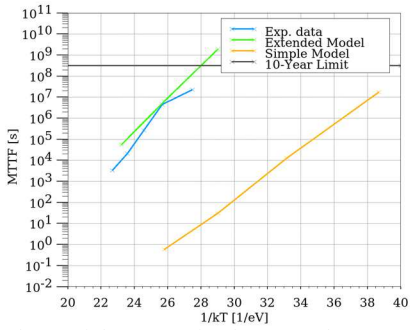

Fig. 12. Temperature dependence of the MTTF for the LRS. The measurements are based on a large collection of type-B samples. A current threshold of 10^{-5}A was used as a failure criterion for LRS. The simple model is found to predict short retention times, while more realistic retention times can be achieved through the extended model. In the latter model, the long retention times are associated with larger barriers for the interface reaction. These barriers can be overcome during SET and RESET phase due to the involvement of the catalyst, while they cause a longer LRS retention, where the electric field across the oxide is small. The larger barriers also result in a stronger temperature dependence of the LRS retention times in the extended model.

Electro-Forming Reaction		Interface Reaction	
k_f	10^{14} s^{-1}	k_f	10^{13} s^{-1}
E_{bf}	0.91 eV	E_{bf}	2.10 eV
k_r	10^{-10} s^{-1}	k_r	10^{-11} s^{-1}
E_{br}	0.18 eV	E_{br}	1.17 eV
p_0 [5,6]	$2.5\cdot10^{-8}$ cm	p_0	$7\cdot10^{-8}$ cm
x	0.54	x	0.5
Other Important Parameters		Extended Bridging Mobility Model	
k [15]	5.0	μ_S	$5\cdot10^{3}$ cm²/(Vs)
κ_{SiOx}[16]	$4\cdot10^{-3}$ W/(cm K)	μ_C	$3.9\cdot10^{-4}$ cm²/(Vs)
C_{SiOx}	2.2 J/(cm³ K)	f_0	0.3
p_1	$4.5\cdot10^{-8}$ cm	δ	0.1
E_d	0.3 eV	E_b	0.125 eV

Table 1. Calibrated parameters used for the electro-forming reaction, the interface reaction, the bridging mobility model, and the lattice heat flow equation in extended ReRAM model. k is the dielectric constant [15], κ_{SiOx} the thermal conductivity [16], C_{SiOx} the heat capacity, and E_d the diffusion barrier of the I_O. It is noted that the dipole moments in the reaction rates remain below $7\cdot10^{-8}$ cm, which is consistent with DFT calculations [17]. In contrast to simulations in other studies [7], we have accounted for the fact that only the fraction x or $1-x$ of the barrier lowering term $z\,\boldsymbol{p_0 E}$ actually affects the forward or reverse reaction barrier. This results to lower effective dipole moments which are compensated by higher values in our simulations.

REFERENCES

[1] A. Mehonic *et al.*, Adv. Mater. **30**, 43, 1801187 (2018).
[2] M. Lanca *et al.*, Adv. Electron. Mater. **5**, 1, 1800143 (2018).
[3] A.Regev *et al.*, AICAS (2020), pp. 145–148.
[4] B. Gao *et al.*, IEDM (2016), pp. 7.3.1–7.3.4.
[5] A. Padovani *et al.*, NVMTS (2017), pp. 1–8.
[6] T. Sadi *et al.*, J.Phys.C: Condens.Matter **30**, 084005 (2018).
[7] A. Makarov *et al.*, IPFA (2010), pp. 1–4.
[8] D. Ielmini, J.Comput.Electron **16**, pp. 1121–1143 (2017).
[9] VICTORY Device User's Manual, Silvaco Intern., 2020.
[10] L. Wu *et al.*, VLSI (2010), pp. 90-91.
[11] V.A. Voronkovskii *et al.*, J.Non-Crystalline Solids **546**, 120256 (2020).
[12] K. Muthuseenu *et al.*, SISPAD (2019), pp. 1–4.
[13] N. Salles *et al.*, Nat Commun **11**, 3330 (2020).
[14] K. Jung *et al.*, IEEE EDL **38**, 6, pp. 728–731 (2017).
[15] S Alexandrova *et al.*, J. Phys.: Conf. Ser. **558** 012054 (2014)
[16] W. Zhu *et al.*, Sci Rep **8**, 10537 (2018).
[17] B.Traoré *et al.*, J.Phys.Chem.C **120**, 43, pp 25023–25029 (2016).

About Silvaco
Silvaco is a leading provider of TCAD, EDA software and semiconductor IP used for process and device development for advanced semiconductors, power IC, display, memory, and SoC design. For over 35 years, Silvaco has enabled its customers to develop next generation semiconductor products in the shortest time with reduced cost. The company is headquartered in Santa Clara, California and has a global presence with offices located in North America, Europe, Japan, China, Taiwan, Korea, and Singapore. https://silvaco.com/

About Weebit Nano
Weebit Nano Ltd. is a leading developer of next-generation semiconductor memory technology. The company's ground-breaking Resistive RAM (ReRAM) addresses the growing need for significantly higher performance and lower power memory solutions in a range of new electronic products such as Internet of Things (IoT) devices, smartphones, robotics, autonomous vehicles, 5G communications and artificial intelligence. Weebit's ReRAM allows semiconductor memory elements to be significantly faster, less expensive, more reliable and more energy efficient than those using existing Flash memory solutions. Because it is based on fab-friendly materials, the technology can be quickly and easily integrated with existing flows and processes, without the need for special equipment or large investments. See: www.weebit-nano.com.